Mechanistic insight into the oligomerisation of *Arabidopsis* CRY1 and its inhibition by BIC1

Alicia Just[1], Nils Niemann[2], Petra Gnau[3], Dennis Kock[2], Thomas Heimerl[4], Lars-Oliver Essen[3], Alfred Batschauer[2] & Nina Morgner[1*]

[1]Institute of Physical and Theoretical Chemistry, Johann Wolfgang Goethe University, Frankfurt/Main, Germany

[2]Department of Biology, Philipps University Marburg, Marburg, Germany

[3]Department of Chemistry, Philipps University Marburg, Marburg, Germany

[4]SYNMIKRO Research Center and Department of Chemistry, Philipps University Marburg, Marburg, Germany

*Corresponding author: Nina Morgner, e-mail: morgner@chemie.uni-frankfurt.de

Abstract

Cryptochromes (CRY) convert blue light signals into biological responses, however, the molecular processes underlying their activation are not fully understood. In this study, we uncover the molecular mechanism underlying the blue-light activation of *Arabidopsis* CRY1 using time-resolved native mass spectrometry combined with kinetic modelling – an approach that allows us to monitor light-driven complex formation with temporal and molecular resolution. We show that CRY1 activation follows a defined, reversible assembly pathway in which monomers rapidly form dimers that then assemble into tetramers. A quantitative two-step model captures the dynamic interplay between light-driven assembly and thermal disassembly. Strikingly, ATP accelerates tetramer formation and stabilises oligomers by tuning the underlying photochemistry of the FAD chromophore. In contrast, the Blue-light Inhibitor of Cryptochromes 1 (BIC1) acts as a potent antagonist. We found that BIC1 binds to CRY1 even in the dark, with a significant increase in binding strength under blue-light conditions. BIC1 not only blocks CRY1 oligomerisation, but also actively dismantles pre-assembled tetramers. This disassembly process is light-independent and occurs regardless of CRY1's redox state. Together, these findings reveal a finely balanced regulatory system in which ATP and BIC1 act as opposing regulators to control CRY1 activation. This work provides a kinetic and mechanistic framework for reversible cryptochrome signalling and highlights how blue light responses can be precisely modulated at the molecular level.

Introduction

Plants rely on light not only as an energy source but also as a critical environmental signal that guides nearly every aspect of their growth and development[1–3]. To perceive and translate light information across the spectrum, plants have evolved a sophisticated network of photoreceptors, including phytochromes, phototropins, the UV-B photoreceptor UVR8, and cryptochromes (CRYs)[1,4–6]. Among these, CRYs are evolutionarily conserved flavoproteins that absorb blue and ultraviolet-A light via a flavin adenine dinucleotide (FAD) chromophore, which is bound non-covalently within the photolyase homology region (PHR) domain[7–10]. The PHR domain is complemented by the cryptochrome C-terminal extension (CCE) that is much less

conserved and varies in length and sequence among cryptochromes[11]. In *Arabidopsis thaliana*, two major cryptochromes, CRY1 and CRY2, operate in partially overlapping but distinct physiological contexts[12]. CRY1 predominantly controls the early seedling stage, where it suppresses hypocotyl elongation, whereas CRY2 regulates flowering time by acting as a photoperiod sensor[12–16]. Activation of plant CRYs is initiated by light-driven photoreduction of FAD[17,18], which induces conformational changes that promote oligomerisation[19–22] and binding to downstream signalling partners[23]. Although CRY1 and CRY2 are structurally related[24], their functional specialization suggests that they may differ in their activation dynamics, signalling interactions, and mechanisms of regulation. Structural studies have demonstrated that both CRY1 and CRY2 undergo blue light–induced oligomerisation[13,15–17], and in the case of CRY2, tetrameric assemblies have been linked to signalling activity[25]. CRY1 likewise forms light-induced oligomers, as revealed by structural analyses[26], yet the dynamics and regulation of this process are poorly understood. While oligomerisation is mediated by the PHR domain, the CCEs are engaged in liquid–liquid phase separation (LLPS)[11]. To distinguish specific oligomerisation from the formation of dynamic size-variable condensates, *in vitro* studies of the isolated PHR domain are essential to uncover the intrinsic mechanism of cryptochrome oligomerisation without the interfering influence of LLPS. In particular, the molecular mechanism underlying CRY1 oligomerisation as well as the influence of cellular cofactors or inhibitory proteins on this process, remains poorly understood.

A major class of negative regulators of CRYs are the Blue-light Inhibitors of Cryptochromes (BICs)[27]. BICs interact with CRY2 in its PHR domain and efficiently block tetramerization, thereby suppressing signalling[21,24]. CRY1 has also been identified as a target of BIC1[21,25–27], but the mechanistic details of this inhibition are not resolved. Previous studies demonstrated that BIC1 may associate with CRY1 in both dark and light conditions[28], raising the question whether BIC1 primarily prevents oligomer formation or whether it can actively dismantle pre-assembled CRY1 complexes.

Another layer of potential regulation arises from cellular metabolites[29–31]. ATP is known to bind the PHR domain of plant cryptochromes[17,18] and a variety of studies reported, that ATP accelerates FAD photoreduction and stabilizes reduced states[30,32–34].

However, whether ATP directly influences CRY1 oligomerisation dynamics has remained unclear.

Building on our previous work, where we demonstrated time-resolved investigation of light-induced conformational changes in the monomeric animal-like cryptochrome from *Chlamydomonas reinhardtii* (*Cr*aCRY)[35], we now take one step further and explore the oligomerisation process that follows photoactivation in CRY1 from *Arabidopsis thaliana*. We combined different native mass spectrometry techniques, absorption spectroscopy and negative-stain transmission electron microscopy, to unravel the light-induced assembly and regulation of *Arabidopsis* CRY1 PHR domain *in vitro*. We show that CRY1 oligomerisation proceeds via a sequential monomer → dimer → tetramer pathway that can be quantitatively described by a reversible two-step kinetic model. ATP accelerates this process, boosting the oligomerisation rates and stabilizing the oligomeric states. Furthermore, we demonstrate that BIC1 binds to CRY1 both in darkness and under blue light illumination, with significantly different affinities. Importantly, BIC1 not only prevents tetramer assembly but also disassembles preformed CRY1 oligomers, a property that extends to the constitutively tetrameric CRY1^{L407F} mutant[36,37]. Finally, we show that BIC1 inhibition does not interfere with photoreduction of the FAD chromophore, indicating that BIC1 regulates CRY1 through direct competition with CRY1-CRY1 contacts rather than through modulation of chromophore photochemistry.

Together, our findings establish a quantitative kinetic framework for CRY1 oligomerisation and reveal dual regulatory inputs: metabolic tuning by ATP and active disassembly by BIC1. These results uncover fundamental principles of CRY1 regulation that distinguish it from CRY2 and highlight new mechanisms by which plant cells integrate metabolic state and the effect of inhibitory proteins to fine-tune cryptochrome signalling.

Results

Oligomerisation mechanism of *Arabidopsis* CRY1. To gain mechanistic insight into *Arabidopsis* CRY1 oligomerisation, we investigated the oligomeric states of the recombinant CRY1 PHR domain (CRY1-PHR), thereafter named CRY1, *in vitro* by

120 nano electrospray ionization mass spectrometry (nESI-MS). Consistent with previous
121 reports[26] CRY1 exists predominantly as a monomer in the dark (m/z = 3500-4800,
122 Fig. 1a) with only a small fraction present as dimers (m/z = 5000-5700). Exposure to
123 blue light promotes its oligomerisation into a tetrameric form (m/z = 6000-8500)
124 (Fig. 1b).

125 To elucidate the underlying mechanism of this light-induced oligomerisation, we next
126 examined whether tetramer assembly occurs exclusively via dimer intermediates or
127 involves trimeric species as transitional state. To address this, we performed time-
128 resolved mass spectrometry at room temperature, allowing us to detect and quantify
129 transient oligomeric species under blue light conditions. The time-resolved data
130 revealed a well-defined kinetic progression of CRY1 oligomerisation (Fig. 1e-g). In the
131 initial dark-adapted state, the cryptochrome was predominantly monomeric
132 (Fig. 1a, e). Upon exposure to blue light, we observed a rapid decrease in monomer
133 abundance (Fig. 1e), accompanied by the appearance of dimers (Fig. 1f). Tetramer
134 formation was observed after a short delay, consistent with a stepwise assembly
135 pathway (Fig. 1g). Dimer levels peaked after approximately 3 seconds (Fig. 1f), while
136 tetramer accumulation progressed more slowly and reached a stationary plateau at
137 120 seconds (Fig. 1g). Notably, the monomeric species did not fully disappear
138 (Fig. 1b, e), suggesting that oligomerisation is opposed by a concurrent thermal
139 dissociation process. This observation shows that even under sustained light
140 activation, reversible oligomer assembly and disassembly are in kinetic competition.

141 To quantitatively describe the oligomerisation mechanism, we propose a reversible
142 kinetic model comprising two steps as shown in Fig. 1l. This kinetic model assumes
143 sequential assembly, from monomer via dimer to tetramer (M→D→T), with no direct
144 conversion from monomer to tetramer and no trimeric species. Fitting our data with
145 this model (Fig. 1e-g, Extended Data Fig. 2a) yielded association and dissociation rate
146 constants listed in Fig. 1k. The model accurately described the experimental time
147 courses of all three oligomeric states at room temperature. The relatively low value of
148 $k_{M\rightarrow D} = (3.7 \pm 0.3) \times 10^{-3}\ \mu M^{-1}\ s^{-1}$ indicates slow dimerization, while the larger
149 association rate $k_{D\rightarrow T} = (75 \pm 4) \times 10^{-3}\ \mu M^{-1}\ s^{-}1$ reflects a more efficient tetramerization
150 step once dimers are present. The dissociation rates further reveal distinct stabilities:
151 the dimer dissociates rapidly with $k_{D\rightarrow M} = (560 \pm 70) \times 10^{-3}\ s^{-1}$, whereas the tetramer
152 is more stable ($k_{T\rightarrow D} = (6.3 \pm 0.6) \times 10^{-3}\ s^{-1}$). Together these rate constants collectively

153 explain the observed accumulation of tetramers and the persistence of monomers in
154 a dynamic light-induced stationary state. These results demonstrate that the
155 experimentally observed oligomerisation dynamics of CRY1 can be effectively
156 described by a two-step reversible reaction model and provide quantitative insight into
157 the kinetics of light-induced assembly.

158

159 **ATP boosts oligomer formation.** Given previous reports that ATP influences the
160 FAD photoreduction kinetics of cryptochromes[30,32–34], we next investigated whether
161 ATP also affects the light-induced oligomerisation of CRY1. Under identical conditions
162 in presence and absence of ATP, we observed a pronounced ATP-dependent
163 enhancement of tetramer formation (Fig. 1c, d). In the presence of 100 µM ATP, CRY1
164 assembled into tetramers more efficiently and reached markedly higher tetramer levels
165 upon blue light exposure (Fig. 1d, Extended Data Fig. 2b). Moreover, the rate of
166 tetramer oligomerisation almost quadrupled, while the subsequent thermal
167 dissociation in darkness was slowed approximately twofold for the tetramer and even
168 more than tenfold for the dimer (Fig. 1h-k). To further assess the concentration
169 dependence of this effect, we also tested a concentration of 200 µM ATP. Under these
170 conditions, we detected a substantial increase in the dimeric CRY1 population already
171 in the dark-adapted state compared to samples without ATP or in presence of 100 µM
172 ATP (Extended Data Fig. 1a-c). This observation suggests that higher ATP
173 concentrations promote or stabilize dimer formation even in the absence of blue light.
174 These findings show that ATP enhances and stabilizes dimer formation, which we
175 observed to be the rate limiting step for tetramer formation under blue light conditions,
176 revealing a broader modulatory role of ATP in tuning cryptochrome oligomerisation
177 dynamics. Absorption spectra also show the boosting effect of ATP on the kinetics of
178 FAD photoreduction, as has already been shown in previous studies[30,32–34]. In our
179 measurements the addition of ATP accelerated the photoreduction of FAD_{ox} to FADH°
180 by approximately 12%, while slowing down the thermal decay of FADH° back to FAD_{ox}
181 by nearly 60% (Extended Data Fig. 1d-h).

182

183 **BIC1 binds CRY1 in both darkness and under blue light.** While BIC1 is known to
184 bind CRY1, it remains unresolved whether this interaction blocks CRY1

oligomerisation or dismantles existing assemblies. We therefore directly investigated the mechanism of CRY1 inhibition by BIC1 using Laser-Induced Liquid Bead Ion Desorption mass spectrometry (LILBID-MS)[38]. In line with the nESI-MS data, LILBID-MS analysis further confirmed that CRY1 exists predominantly as a monomer in the dark (~ 59 kDa), with only a minor dimeric population (~ 120 kDa) detectable (Fig. 2a). Blue-light illumination shifted the oligomeric distribution rapidly toward tetrameric assemblies (~ 240 kDa), underscoring light-dependent higher-order organization of CRY1 (Fig. 2b). A small trimeric CRY1 population was also detected, arising from partial dissociation of the tetramer induced by the energy input during LILBID-MS analysis (Extended Data Fig. 3a). Upon addition of BIC1 (~ 20 kDa) in both the dark and under blue light conditions, we observed a discrete charge distribution corresponding to the mass of CRY1-BIC1 heterodimer (~ 79 kDa), indicating direct binding between the two proteins (Fig. 2c, d). While CRY1 exhibited reduced binding to BIC1 in the dark (Fig. 2c), we observed a significant increase in CRY1-BIC1 heterodimer formation under blue light conditions (Fig. 2d). Notably, in light-exposed samples, the CRY1 tetramer signal was absent, suggesting that BIC1 binding prevents oligomer formation. To quantify the interaction strength of CRY1-BIC1 heterodimer in the dark and under blue light conditions, we employed quantitative LILBID-MS (qLILBID-MS), a label-free technique capable of measuring dissociation constants under native-like conditions[39,40]. In the dark, BIC1 bound CRY1 with moderate affinity ($K_D \approx 1.2$ µM) (Fig. 2g), whereas under blue light, the interaction became more stable ($K_D \approx 0.13$ µM) (Fig. 2f). This ten-fold increase in affinity suggests that light-induced conformational changes in CRY1 enhance its recognition by BIC1. This demonstrates that BIC1 binds CRY1 in both its inactive and active state but with a strong preference for the light-activated form, consistent with a mechanism in which BIC1 selectively inhibits photoactivated CRY1.

BIC1 reverses CRY1 oligomerisation. Given that CRY1 tetramerizes upon blue light exposure (Fig. 2b), and that BIC1 binds with high affinity under blue light (Fig. 2d), the question arises whether BIC1 merely blocks tetramer formation or can even actively dismantle pre-existing CRY1 oligomers as it was shown for CRY2 and BICs[21,24]. Therefore, we added BIC1 to pre-illuminated, tetrameric CRY1 under constant illumination with blue light. The mass spectra indicate that BIC1 binds sequentially to

218 individual CRY1 protomers within the tetramer (~ 260-320 kDa) (Fig. 2e), displacing
219 them from the tetrameric complex and a formation of a dominant BIC1–CRY1
220 heterodimer (~ 79 kDa). These data suggest that BIC1 not only prevents tetramer
221 formation but also actively dismantles existing CRY1 tetramers by occupying all
222 subunits.

223 Negative-stain transmission electron microscopy (TEM) corroborates the mass
224 spectrometry data. In blue light-treated samples, CRY1 formed doughnut-like ring
225 structures that were absent in dark-adapted preparations (Fig. 2h, i), consistent with
226 the formation of tetrameric assemblies. The addition of BIC1 markedly reduced the
227 abundance of these oligomeric particles. Even immediately after 30 minutes of
228 illumination, CRY1 samples incubated with BIC1 displayed few ring-like structures
229 (Fig. 2k). Moreover, following transfer to darkness, CRY1 oligomers disassembled
230 significantly faster in the presence of BIC1, with near-complete monomerization
231 observed at the earliest time point (Fig. 2j).

232 **BIC1 disassembles CRY1 tetramers independently of light activation.** To
233 examine whether BIC1-mediated inhibition of CRY1 tetramers requires light activation,
234 we analyzed the CRY1^{L407F} mutant, which has been observed to be hyperactive and
235 results in a constitutive photomorphogenic phenotype[36,37]. Analytical size exclusion
236 chromatography (SEC) revealed, that CRY1^{L407F} shows already a tetrameric retention
237 time in darkness compared to the wild-type CRY1 (Fig. 3d). LILBID-MS confirmed the
238 presence of tetramers for CRY1^{L407F} in darkness (Fig. 3a) and absorption
239 spectroscopy has shown that the leucine to phenylalanine replacement at position 407
240 does not impair photoreduction of the chromophore (Fig. 3h).

241 Upon addition of BIC1, the CRY1^{L407F} tetramers were efficiently disassembled into
242 BIC1–CRY1^{L407F} heterodimers (Fig. 3b, Extended Data Fig. 3b). In contrast to the wild-
243 type CRY1 (Fig. 2c, d), exposure to blue light did not further enhance the formation of
244 the CRY1^{L407F}-BIC1 heterodimer (Fig. 3c) or have any other significant effect on the
245 observed complexes. qLILBID measurements revealed that BIC1 binds CRY1^{L407F}
246 independently of illumination with high affinity (K_D = 0.10 ± 0.03 µM), comparable to
247 the affinity of BIC1 for light-activated wild-type CRY1 (K_D = 0.13 ± 0.09 µM). This
248 result demonstrates that the L407F mutation induces a conformational change in
249 CRY1 that mimics its light-activated state with respect to BIC1 recognition.

250 Collectively, these findings suggest that BIC1 disrupts CRY1 oligomerisation by
251 binding individual CRY1 protomers with higher affinity than the protomer-protomer
252 interactions, effectively outcompeting CRY1-CRY1 contacts regardless of the
253 photoreduction state of the chromophore.

254

255 **BIC1 does not inhibit photoreduction of the CRY1 FAD cofactor.** The remaining
256 open question is whether BIC1 suppresses CRY1 oligomerisation by interfering with
257 its photoactivation, as previously demonstrated for CRY2 inhibition by BIC2[24]. To
258 address this, we examined the photoreduction state of the FAD chromophore in the
259 presence and absence of BIC1. Absorption spectra of purified CRY1 recorded before
260 and after blue light exposure showed the expected spectral changes associated with
261 FAD photoreduction (Fig. 3f, Extended Data Fig. 1d, e). In the dark-adapted state,
262 CRY1 displayed absorption maxima characteristic of oxidized flavin (FAD_{ox}) at 450 nm
263 and a shoulder near 480 nm. Upon blue light illumination, these peaks decreased in
264 intensity, accompanied by the appearance of a broad band between 550-600 nm,
265 consistent with the formation of the neutral semiquinone radical (FADH°)[17,18,41]. These
266 spectral changes are characteristic for the light-driven redox transition of the CRY1
267 chromophore. Identical spectral features were observed when CRY1 or $CRY1^{L407F}$
268 were incubated with BIC1 under the same conditions (Fig. 3g, i, Extended Data
269 Fig. 4a-c), indicating that BIC1 does not impair the light-induced redox transition of the
270 FAD_{ox} to FADH°. This suggests that BIC1 does not block the initial photoactivation
271 step of CRY1. Instead, it acts downstream of photoreduction, targeting the light-
272 induced oligomeric states of CRY1.

273

274 Discussion

275 Light perception in plants is a dynamic process influenced by multiple molecular
276 factors. Our kinetic analysis of CRY1 reveals that oligomerisation proceeds through
277 discrete assembly steps and is modulated by both metabolic signals and inhibitory
278 interactions. These findings suggest that CRY1 activity can be finely adjusted in
279 response to changing conditions, enabling a more nuanced regulation of light
280 signalling.

281 Our time-resolved native mass spectrometry data establish a clear kinetic pathway for
282 CRY1 oligomerisation (Fig. 4). The sequential monomer-to-dimer-to-tetramer
283 assembly we observed is consistent with a two-step reversible kinetic model (Fig. 1l),
284 identifying dimer formation as the rate-limiting step in CRY1 activation. In comparison,
285 FAD photoreduction occurs within microseconds[42], much faster than oligomerisation,
286 indicating that the light-induced activation of the flavin cofactor does not contribute any
287 significant kinetic delay. The relative stabilities of the oligomers differ substantially,
288 with dimers being highly transient while tetramers display significantly increased
289 stability. These light dependent equilibria, suggests that CRY1 signalling is a highly
290 dynamic process rather than a simple on-off switch. To directly compare our *in vitro*
291 oligomerisation kinetics with *in vivo* observations made by Liu *et al*. (2020)[22], we fitted
292 the tetramer formation data using a single-exponential model and determined a half-
293 life of approximately $t_{1/2}$ = 18 s (Extended Data Fig. 2c). *In vivo*, the corresponding
294 half-life at a fluence rate of 30 µmol m^{-2} s^{-1} is about five times longer, reflecting
295 additional cellular constraints such as regulatory interactions (e. g. BIC1 inhibition),
296 metabolites, different reducing environment, temperature and, of course, different
297 protein concentrations. Despite these differences, the timescales remain within the
298 same order of magnitude, underscoring the physiological relevance of the
299 oligomerisation process captured by time-resolved mass spectrometry. Importantly,
300 our *in vitro* approach allows disentangling the influence of individual factors that cannot
301 easily be resolved in the cellular context, thereby complementing *in vivo*
302 measurements. Beyond this biological relevance, such a detailed kinetic analysis also
303 opens opportunities for engineering CRY1-based optogenetic tools with tuneable
304 temporal precision, complementing existing CRY2-based optogenetic systems[43–46].

305 In addition to intrinsic kinetic insights, our findings highlight how cellular metabolites
306 can modulate this process. We show that ATP dramatically enhances CRY1
307 oligomerisation upon illumination (Fig. 4). Increasing ATP concentrations significantly
308 enhance the formation of CRY1 dimer (Extended Data Fig. 1a-c) which we showed to
309 be the rate limiting step in oligomer assembly. Then tetramer formation proceeds
310 rapidly, resulting in more stable higher-order oligomers.

311 This is particularly intriguing given that ATP is not only a fundamental energy currency
312 but has also been reported to bind the PHR domain of plant cryptochromes[21,28] and
313 affect FAD photoreduction kinetics[30,32–34]. Our data support the notion that ATP acts

314 as a cofactor, stabilizing the oligomeric state and promoting the conformational
315 changes required for stable oligomer formation. This mechanism suggests a novel link
316 between the cellular energy status and CRY1 activity, allowing a plant to modulate its
317 light response in accordance with its metabolic state. For instance, it is conceivable
318 that under conditions of high energy availability, CRY1 signalling may be sensitized to
319 support energy-intensive processes such as development and growth.

320 Our data further elucidate the inhibitory role of BIC1, revealing an elegant mechanism
321 of regulation (Fig. 4). We demonstrate that BIC1 binds to CRY1 in both dark and light
322 conditions (Fig. 2c, d), but with an enhanced affinity for the light-activated form
323 (Fig. 2f, g). This light-dependent increase in binding affinity indicates that light-induced
324 conformational changes in CRY1 significantly promote its interaction with BIC1. This
325 light-dependent increase in affinity is a crucial finding, as it provides a mechanism for
326 the selective inhibition of active CRY1. Moreover, we provide clear evidence that BIC1
327 is an active disassembler of CRY1 oligomers, rather than just a passive competitor
328 (Fig. 2e). Given that the constitutively active $CRY1^{L407F}$ mutant, which mimics the
329 tetrameric light-activated state, shows a high affinity for BIC1 (Fig. 3e), strongly
330 suggests that BIC1 recognizes a specific conformational state of CRY1, independent
331 of the FAD redox state. Our result that BIC1 does not interfere with FAD
332 photoreduction (Fig. 3g, i) differs from recent reports on the CRY2-BIC2 interaction[24],
333 suggesting that the inhibitory mechanisms are distinct for CRY1 and CRY2. This
334 supports the idea that while cryptochromes share a conserved photochemical
335 activation step, their downstream regulation can vary, allowing for functional
336 specificity.

337 In summary, our work establishes a quantitative kinetic model for CRY1
338 oligomerisation. By showing that ATP acts as an oligomerisation accelerator and BIC1
339 as an active disassembler, we provide a more detailed and nuanced understanding of
340 how CRY1 activity is regulated beyond simple light perception. These insights not only
341 shed light on the functional specialization of CRY1 but also highlight a broader
342 principle of plant signalling, where a photoreceptor's output is shaped by a complex
343 interplay between light, metabolites, and dedicated regulatory proteins.

344

345 # Methods

346 **Cloning of constructs**. The expression vectors encoding the PHR domain (residues
347 1–509) of *Arabidopsis thaliana* CRY1 and the CRY1^{L407F} mutant, both cloned into the
348 pACYCDuet-1 vector have been described previously[26]. To prevent disulfide bond-
349 mediated dimerization observed in the *Arabidopsis thaliana* wild-type BIC1 protein
350 (Extended Data Fig. 5a, b), a synthetic gene encoding a BIC1 variant carrying three
351 cysteine-to-alanine substitutions (C99A, C105A, C136A) was generated. This triple
352 mutant, named BIC1 throughout the text, was synthesized and cloned into the
353 pET28a(+) vector (*BioCat GmbH*). Recombinant proteins carried an N-terminal His_6-
354 tag.

355 **Overproduction and purification of recombinant proteins**. For overexpression of
356 CRY1 and the CRY1^{L407F} mutant as well as BIC1^{3CA}, competent *E. coli* BL21 Star
357 (DE3) cells (*Thermo Fisher*) were used. For CRY1 and CRY1^{L407F} overproduction,
358 20 mL overnight cultures were inoculated into 2 L LB medium supplemented with
359 34 µg/mL chloramphenicol in 5 L baffled flasks. Cultures were incubated at 37 °C with
360 shaking (110 rpm) until an $OD_{600\ nm}$ of ~1.0 was reached. Cells were placed on ice for
361 30 min, and expression was induced with 0.25 mM IPTG. All further steps were carried
362 out under red light. Cultures were incubated for 3 days at 16 °C. Cells were harvested
363 by centrifugation (5,330g, 15 min, 4 °C) and resuspended in lysis buffer (50 mM
364 MOPS, pH 7.4, 300 mM NaCl, 10% glycerol, 1% Triton X-100). Lysozyme (0.2 mg/mL),
365 PMSF (0.4 mM) and DNase I were added, and the suspensions were incubated for
366 10 min at room temperature before disruption using a French press. Lysates were
367 clarified by centrifugation (39,000g, 30 min) and filtered. The supernatant was applied
368 onto a 1 mL Protino Ni-NTA column (*Macherey-Nagel*), followed by sequential
369 washing steps with lysis buffer, buffer containing 3% Triton X-100, and lysis buffer
370 without TX-100 until a stable UV baseline was reached. Non-specifically bound
371 proteins were removed with 10% elution buffer (50 mM MOPS, pH 7.4, 300 mM NaCl,
372 10% glycerol, 250 mM imidazole). Recombinant CRYs were eluted with 100% elution
373 buffer. CRY1 concentrations were kept below 1 mg/mL to prevent oligomerisation.
374 Final purification was performed by size-exclusion chromatography (Superdex 200 pg
375 16/60, *Cytiva*).

376 BIC1 purification followed a similar protocol. Expression was induced with 0.5 mM
377 IPTG, and cultures were incubated for 18 h at 25 °C. Cells were harvested, washed
378 with PBS, and resuspended in lysis buffer (50 mM HEPES, pH 7.0, 500 mM NaCl, 10%
379 glycerol). Cell disruption was performed as described above, using a protease inhibitor
380 mix (*Carl Roth, Cat. no. 3760.1*) in place of PMSF. The soluble fraction was loaded
381 onto a Ni-NTA column and washed with protein buffer (50 mM HEPES, pH 7.0,
382 300 mM NaCl, 10% glycerol), followed by a wash containing 3% Triton X-100 and
383 protein buffer. Additional washes were performed with 10% and 20% elution buffer
384 (50 mM HEPES, pH 7.0, 300 mM NaCl, 250 mM imidazole, 10% glycerol). BIC1 was
385 eluted with 100% elution buffer, concentrated, and further purified via size-exclusion
386 chromatography (Superdex 75 pg 16/60, *Cytiva*).

387 **Size exclusion chromatography (SEC).** For analysis of blue light-dependent
388 oligomerisation, samples containing 30 µM CRY1 and 10 mM ß-mercaptoethanol in
389 100 µl volumes were separated on a Superdex 200 10/300 GL column (*GE*
390 *Healthcare*) equilibrated at 10 °C in buffer D containing 20 mM ß-mercaptoethanol.
391 CRY1 was pre-illuminated with blue light (465 ± 5 nm, 115 µmol m^{-2} s^{-1}) for 20 min.
392 Three blue light LEDs were used to illuminate the column resin. Dark controls were
393 kept in red safe light. Calibration of the column was done using gel-filtration standards
394 (*Sigma Aldrich*).

395 **Photoreduction and dark reversion of CRY1.** Absorbance changes of bound flavin
396 were measured by UV-Vis spectroscopy (*Specord 600, Analytik Jena*). Before
397 photoreduction, the CRY1 solution was centrifuged (10 min, 16873 g, 4 °C) to pellet
398 and remove aggregated protein. A protein solution of 10 µM CRY1 was prepared, and
399 dithiothreitol (DTT) added to a final concentration of 10 mM. For photoreduction,
400 samples were irradiated with a 455 nm LED (M455L2, *Thorlabs*) at 100 µmol m^{-2} s^{-1}.
401 At defined time points, the absorption between 200 nm – 900 nm was recorded. The
402 dark conversion was monitored with the same photoreduced sample by leaving it in
403 the dark until full recovery and absorbance recording. During all steps, cuvettes were
404 chilled at 20 °C.

405 **Nano Electrospray ionization mass spectrometry.** nESI-MS was carried out using
406 a Synapt G2-S instrument (*Waters Corporation, Wilmslow, UK*) equipped with a high-
407 mass quadrupole modification. Nano electrospray emitters are produced in-house by

408 pulling borosilicate glass capillaries with a Flaming/Brown micropipette puller (P-1000,
409 *Sutter Instrument Co.*) and subsequently coated with a gold layer via sputtering. CRY1
410 (15 μM) was analyzed at room temperature in positive ion mode under a capillary
411 voltage of 1.1 kV. The ion source was operated with a cone voltage of 150 V, an offset
412 of 100 V, and maintained at 20 °C. The scan time was set to 1 scan per second.
413 Calibration is performed using a standard cesium iodide (CsI) solution. Sample
414 illumination was carried out by irradiation of the nano electrospray emitters with a
415 455 nm LED (M455L4, *Thorlabs*) at 30-50 μmol m^{-2} s^{-1} (Extended Data Fig. 6a), using
416 an illumination setup similar to that described by Camacho *et al*. (2019).[47] Acquisition
417 and data processing are achieved using MassLynx™ V4.1 SCN901. Prior to
418 measurements, CRY1 was buffer-exchanged in 200 mM ammonium acetate, 10 mM
419 DTT and pH 7.4, using Zeba Micro Spinbuffer exchangers (7 kDa MWCO, *Thermo*
420 *Fisher Scientific*).

421 **nESI-MS based rate constant determination.** The measurements of the rate
422 constants were performed following the same procedure as for the nESI-MS
423 measurements except for the scan time, which was set to 10 scans per second. The
424 intensity (counts) of each species (monomer, dimer, tetramer) during the
425 measurement period was estimated by generating an extracted ion chromatogram
426 using MassLynx™ V4.1 SCN901. Initial concentrations of each species (monomer,
427 dimer, tetramer) were determined from the measured signal intensities, assuming a
428 total sample concentration of 15 μM relative to the molecular mass of the monomer.
429 Kinetic data were analyzed by using DynaFit[48] software and a reversible two-step
430 kinetic model (Fig. 1l) based on the differential equations 1-3.

$$\frac{d[M]}{dt} = -2k_{M\to D}[M][M] + 2k_{D\to M}[D] \quad (1)$$

$$\frac{d[D]}{dt} = +k_{M\to D}[M][M] - k_{D\to M}[D] - 2k_{D\to T}[D][D] + 2k_{T\to D}[T] \quad (2)$$

$$\frac{d[T]}{dt} = +k_{D\to T}[D][D] - k_{T\to D}[T] \quad (3)$$

431

432 **LILBID-MS.** Prior to analysis by LILBID-MS[38], CRY1 and BIC1[3CA] were buffer-
433 exchanged as described for nESI-MS. All measurements were performed at 20 °C,
434 using 4 μL of buffer-exchanged and degassed sample for each analysis. Microdroplets

435 with a diameter of 50 µm are generated using a piezo-driven droplet generator (MD-
436 K-130, *Microdrop Technologies GmbH,* Norderstedt, Germany) operating at 10 Hz.
437 The droplets are transferred into a vacuum of about 10^{-5} mbar and irradiated with a
438 pulsed infrared laser (*Innolas Spitlight 400, Continuum PowerLite 8000*) tuned to the
439 vibrational absorption maximum of water (2.8 µm). Absorption of laser energy (10-
440 23 mJ per pulse) by water molecules causes an explosive expansion of the droplets,
441 resulting in the release of analyte ions into the gas phase. The ions are accelerated
442 using a pulsed electric field and analysed with a home-built time-of-flight mass
443 spectrometer in negative ion mode. Each mass spectrum represents an average
444 signal from 1,000 individual microdroplets. Mass spectra are calibrated against a
445 10 µM aqueous bovine serum albumin standard and subsequently processed by
446 smoothing and background subtraction. The sample was exposed to blue light
447 (455 nm LED, M455L4, *Thorlabs*) at 100 µmol m^{-2} s^{-1} inside the droplet generator via
448 a coupled optical fibre that was installed on the generator (Extended Data Fig. 6b).

449 For qLILBID-MS[39,40] experiments the laser energy transferred into the droplets is
450 correlated to the degree of complex dissociation. Therefore, the explosion of the
451 irradiated droplets is visualized by illuminating the explosion with a green laser (Minilite
452 I, *Continuum*, San Jose, USA) and the resulting images are captured using a high-
453 speed camera (DFK 23UP031, *Imaging Source*, Bremen, Germany). Each individual
454 droplet yields both a mass spectrum and a corresponding image of the explosion. The
455 explosion width for each droplet is determined by analysing the recorded images with
456 OpenCV, using a custom written Python script. The resulting dissociation plots allow
457 K_D determination.

458 **TEM negative staining.** Carbon coated copper grids (400 mesh) were hydrophilized
459 by glow discharging (*PELCO easiGlow*, Ted Pella, USA). 5 µl of a protein suspension
460 with a concentration of 30 µg/ml was applied onto the hydrophilized grids and stained
461 with 2% uranyl acetate after a short washing step with filtered H_2O_{bidest}. If applicable,
462 samples were prepared under blue (465 ± 5 nm, 115 µmol $m^{-2}s^{-1}$) or safe red light,
463 respectively. Samples were analysed with a JEOL JEM-2100 transmission electron
464 microscope using an acceleration voltage of 120 kV. For image acquisition a F214
465 FastScan CCD camera (*TVIPS, Gauting*) was used.

466

467 ## Data Availability

468 All data generated in this study are provided as Source Data with this paper. Gene
469 accessions codes are At3G52740 (*BIC1*) and At4G08920 (*CRY1*).

470

471 ## References

472 1. Franklin, K. A., Larner, V. S. & Whitelam, G. C. The signal transducing
473 photoreceptors of plants. *Int. J. Dev. Biol.* **49**, 653–664 (2005).
474 2. Halliday, K. J., Martínez-García, J. F. & Josse, E.-M. Integration of Light and Auxin
475 Signaling. *Cold Spring Harb. Perspect. Biol.* **1**, a001586 (2009).
476 3. Heijde, M. & Ulm, R. UV-B photoreceptor-mediated signalling in plants. *Trends*
477 *Plant Sci.* **17**, 230–237 (2012).
478 4. Fankhauser, C. The Phytochromes, a Family of Red/Far-red Absorbing
479 Photoreceptors *. *J. Biol. Chem.* **276**, 11453–11456 (2001).
480 5. Christie, J. M. & Briggs, W. R. Blue Light Sensing in Higher Plants *. *J. Biol.*
481 *Chem.* **276**, 11457–11460 (2001).
482 6. Yadav, A. *et al.* Light signaling and UV-B-mediated plant growth regulation. *J.*
483 *Integr. Plant Biol.* **62**, 1270–1292 (2020).
484 7. Lin, C. *et al.* Association of Flavin Adenine Dinucleotide with the *Arabidopsis* Blue
485 Light Receptor CRY1. *Science* **269**, 968–970 (1995).
486 8. Malhotra, K., Kim, S.-T., Batschauer, A., Dawut, L. & Sancar, A. Putative Blue-
487 Light Photoreceptors from Arabidopsis thaliana and Sinapis alba with a High
488 Degree of Sequence Homology to DNA Photolyase Contain the Two Photolyase
489 Cofactors but Lack DNA Repair Activity. *Biochemistry* **34**, 6892–6899 (1995).
490 9. Brautigam, C. A. *et al.* Structure of the photolyase-like domain of cryptochrome 1
491 from Arabidopsis thaliana. *Proc. Natl. Acad. Sci.* **101**, 12142–12147 (2004).

492 10. Hanić, M. *et al.* Dimerization of European Robin Cryptochrome 4a. *J. Phys.*
493 *Chem. B* **127**, 6251–6264 (2023).
494 11. Wang, X. & Lin, C. The two action mechanisms of plant cryptochromes.
495 *Trends Plant Sci.* **30**, 775–791 (2025).
496 12. Yang, Z. *et al.* Cryptochromes Orchestrate Transcription Regulation of
497 Diverse Blue Light Responses in Plants. *Photochem. Photobiol.* **93**, 112–127
498 (2017).
499 13. Ahmad, M. & Cashmore, A. R. HY4 gene of A. thaliana encodes a protein with
500 characteristics of a blue-light photoreceptor. *Nature* **366**, 162–166 (1993).
501 14. Guo, H., Yang, H., Mockler, T. C. & Lin, C. Regulation of Flowering Time by
502 Arabidopsis Photoreceptors. *Science* **279**, 1360–1363 (1998).
503 15. Wang, J., Du, X., Pan, W., Wang, X. & Wu, W. Photoactivation of the
504 cryptochrome/photolyase superfamily. *J. Photochem. Photobiol. C Photochem.*
505 *Rev.* **22**, 84–102 (2015).
506 16. Wang, Q. & Lin, C. Mechanisms of Cryptochrome-Mediated Photoresponses
507 in Plants. *Annu. Rev. Plant Biol.* **71**, 103–129 (2020).
508 17. Bouly, J.-P. *et al.* Cryptochrome Blue Light Photoreceptors Are Activated
509 through Interconversion of Flavin Redox States*. *J. Biol. Chem.* **282**, 9383–9391
510 (2007).
511 18. Banerjee, R. *et al.* The Signaling State of Arabidopsis Cryptochrome 2
512 Contains Flavin Semiquinone *. *J. Biol. Chem.* **282**, 14916–14922 (2007).
513 19. Sang, Y. *et al.* N-Terminal Domain–Mediated Homodimerization Is Required
514 for Photoreceptor Activity of Arabidopsis CRYPTOCHROME 1. *Plant Cell* **17**,
515 1569–1584 (2005).

516 20. Rosenfeldt, G., Viana, R. M., Mootz, H. D., von Arnim, A. G. & Batschauer, A.
517 Chemically Induced and Light-Independent Cryptochrome Photoreceptor
518 Activation. *Mol. Plant* **1**, 4–14 (2008).
519 21. Wang, Q. *et al.* Photoactivation and inactivation of Arabidopsis cryptochrome
520 2. *Science* **354**, 343–347 (2016).
521 22. Liu, Q. *et al.* Photooligomerization Determines Photosensitivity and
522 Photoreactivity of Plant Cryptochromes. *Mol. Plant* **13**, 398–413 (2020).
523 23. Ponnu, J. & Hoecker, U. Signaling Mechanisms by Arabidopsis
524 Cryptochromes. *Front. Plant Sci.* **13**, 844714 (2022).
525 24. Ma, L. *et al.* Structural insights into BIC-mediated inactivation of Arabidopsis
526 cryptochrome 2. *Nat. Struct. Mol. Biol.* **27**, 472–479 (2020).
527 25. Palayam, M. *et al.* Structural insights into photoactivation of plant
528 Cryptochrome-2. *Commun. Biol.* **4**, 28 (2021).
529 26. Shao, K. *et al.* The oligomeric structures of plant cryptochromes. *Nat. Struct.*
530 *Mol. Biol.* **27**, 480–488 (2020).
531 27. Wang, X. *et al.* A CRY–BIC negative-feedback circuitry regulating blue light
532 sensitivity of Arabidopsis. *Plant J. Cell Mol. Biol.* **92**, 426–436 (2017).
533 28. Miao, L. *et al.* Arabidopsis cryptochrome 1 undergoes COP1 and LRBs-
534 dependent degradation in response to high blue light. *New Phytol.* **234**, 1347–
535 1362 (2022).
536 29. El-Esawi, M. *et al.* Cellular metabolites modulate in vivo signaling of
537 Arabidopsis cryptochrome-1. *Plant Signal. Behav.* **10**, e1063758 (2015).
538 30. Engelhard, C. *et al.* Cellular metabolites enhance the light sensitivity of
539 Arabidopsis cryptochrome through alternate electron transfer pathways. *Plant Cell*
540 **26**, 4519–4531 (2014).

541 31. Zhao, X. *et al.* A Study of Gibberellin Homeostasis and Cryptochrome-
542 Mediated Blue Light Inhibition of Hypocotyl Elongation. *Plant Physiol.* **145**, 106–
543 118 (2007).
544 32. Immeln, D., Schlesinger, R., Heberle, J. & Kottke, T. Blue Light Induces
545 Radical Formation and Autophosphorylation in the Light-sensitive Domain of
546 *Chlamydomonas* Cryptochrome*. *J. Biol. Chem.* **282**, 21720–21728 (2007).
547 33. Müller, P. *et al.* ATP Binding Turns Plant Cryptochrome Into an Efficient
548 Natural Photoswitch. *Sci. Rep.* **4**, 5175 (2014).
549 34. Eckel, M., Steinchen, W. & Batschauer, A. ATP boosts lit state formation and
550 activity of Arabidopsis cryptochrome 2. *Plant J.* **96**, 389–403 (2018).
551 35. Zangl, R. *et al.* Time-Resolved Ion Mobility Mass Spectrometry to Solve
552 Conformational Changes in a Cryptochrome. *J. Am. Chem. Soc.* **146**, 14468–
553 14478 (2024).
554 36. Exner, V. *et al.* A Gain-of-Function Mutation of Arabidopsis
555 CRYPTOCHROME1 Promotes Flowering. *Plant Physiol.* **154**, 1633–1645 (2010).
556 37. Orth, C., Niemann, N., Hennig, L., Essen, L.-O. & Batschauer, A. Hyperactivity
557 of the Arabidopsis cryptochrome (cry1) L407F mutant is caused by a structural
558 alteration close to the cry1 ATP-binding site. *J. Biol. Chem.* **292**, 12906–12920
559 (2017).
560 38. Peetz, O. *et al.* LILBID and nESI: Different Native Mass Spectrometry
561 Techniques as Tools in Structural Biology. *J. Am. Soc. Mass Spectrom.* **30**, 181–
562 191 (2019).
563 39. Schulte, J., Tants, J.-N., von Ehr, J., Schlundt, A. & Morgner, N.
564 Determination of dissociation constants via quantitative mass spectrometry. *Front.*
565 *Anal. Sci.* **3**, (2023).

566 40. Young, P., Hense, G., Immer, C., Wöhnert, J. & Morgner, N. LILBID laser
567 dissociation curves: a mass spectrometry-based method for the quantitative
568 assessment of dsDNA binding affinities. *Sci. Rep.* **10**, 20398 (2020).
569 41. Liu, H., Zhong, D. & Lin, C. Searching for a photocycle of the cryptochrome
570 photoreceptors. *Curr. Opin. Plant Biol.* **13**, 578–586 (2010).
571 42. Langenbacher, T., Immeln, D., Dick, B. & Kottke, T. Microsecond Light-
572 Induced Proton Transfer to Flavin in the Blue Light Sensor Plant Cryptochrome. *J.*
573 *Am. Chem. Soc.* **131**, 14274–14280 (2009).
574 43. Taslimi, A. *et al.* An optimized optogenetic clustering tool for probing protein
575 interaction and function. *Nat. Commun.* **5**, 4925 (2014).
576 44. Che, D. L., Duan, L., Zhang, K. & Cui, B. The Dual Characteristics of Light-
577 Induced Cryptochrome 2, Homo-oligomerization and Heterodimerization, for
578 Optogenetic Manipulation in Mammalian Cells. *ACS Synth. Biol.* **4**, 1124–1135
579 (2015).
580 45. Park, H. *et al.* Optogenetic protein clustering through fluorescent protein
581 tagging and extension of CRY2. *Nat. Commun.* **8**, 30 (2017).
582 46. Hallett, R. A., Zimmerman, S. P., Yumerefendi, H., Bear, J. E. & Kuhlman, B.
583 Correlating in Vitro and in Vivo Activities of Light-Inducible Dimers: A Cellular
584 Optogenetics Guide. *ACS Synth. Biol.* **5**, 53–64 (2016).
585 47. Camacho, I. S. *et al.* Native mass spectrometry reveals the conformational
586 diversity of the UVR8 photoreceptor. *Proc. Natl. Acad. Sci.* **116**, 1116–1125
587 (2019).
588 48. Kuzmic, P. Program DYNAFIT for the analysis of enzyme kinetic data:
589 application to HIV proteinase. *Anal. Biochem.* **237**, 260–273 (1996).

Acknowledgements

We thank Konstantinos Stamatakis for his support and fruitful discussions during the kinetic modelling process, and Josef Wachtveitl for providing access to the absorption spectrometer. We also acknowledge Jeanette Schermuly for technical assistance and Stephan Kiontke for his contributions to the recombinant expression of BIC1 and for helpful discussions. Funding was provided by the German Research Foundation (DFG): A.J. was supported through the Collaborative Research Center CRC 1507 “Membrane-Associated Protein Assemblies, Machineries and Supercomplexes”, N.M. through DFG Grant 557111829, L.-O.E. through DFG grant ES152/18 and A.B. through DFG grant BA985/15-1.

Author contributions

A.J., N.M., L.-O.E., A.B. designed and coordinated the experiments. P.G., A.J., N.N. and D.K. expressed and purified the proteins. A.J. performed mass spectrometry, UV-Vis spectroscopy and kinetic modelling. N.N. and T.H. acquired and interpreted the TEM data. N.N. acquired and interpreted the SEC data. A.J. wrote the original draft. A.J., N.M., A.B., P.G., L.-O.E. edited the manuscript.

Competing interests

The authors declare no competing interests.

Figures and Legends

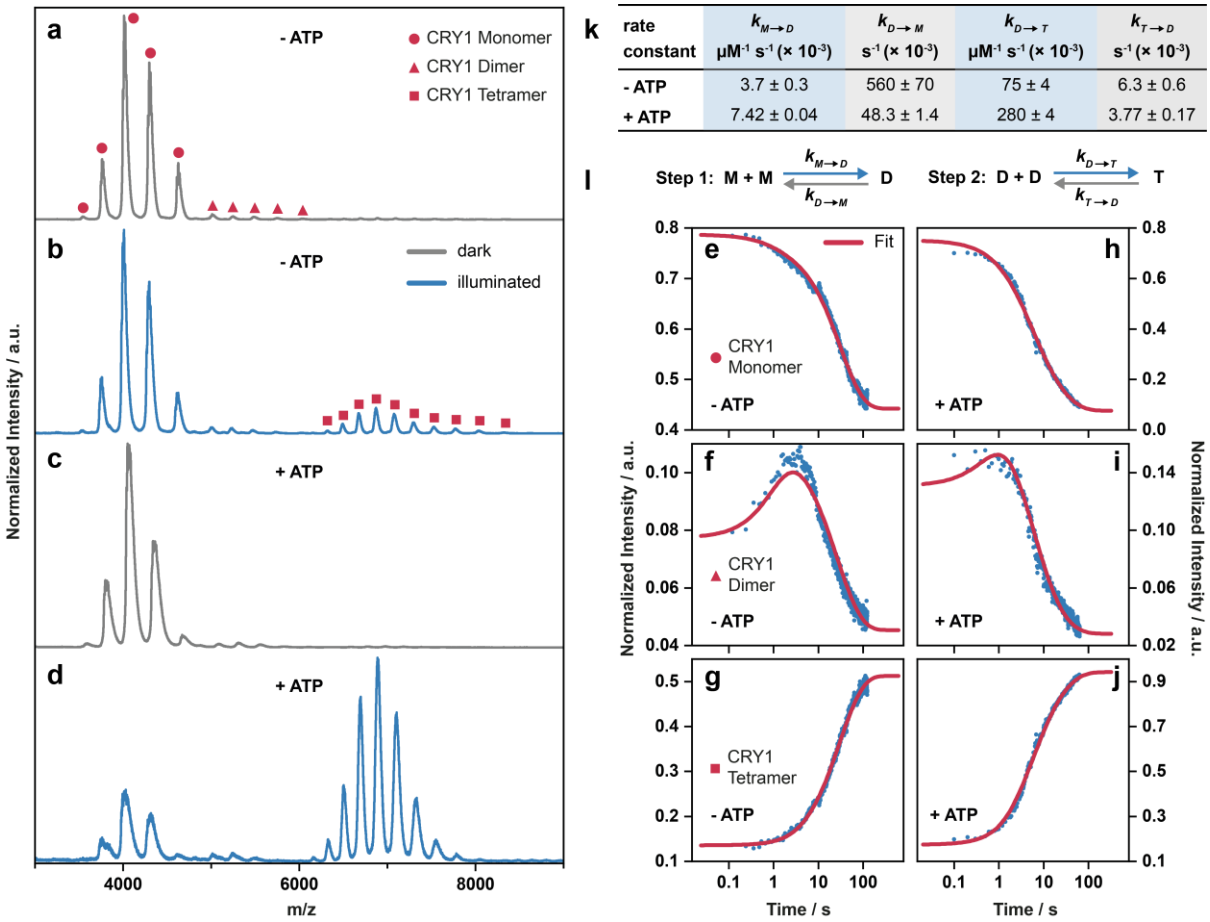

rate constant	$k_{M\rightarrow D}$ $\mu M^{-1}\ s^{-1}$ ($\times 10^{-3}$)	$k_{D\rightarrow M}$ s^{-1} ($\times 10^{-3}$)	$k_{D\rightarrow T}$ $\mu M^{-1}\ s^{-1}$ ($\times 10^{-3}$)	$k_{T\rightarrow D}$ s^{-1} ($\times 10^{-3}$)
- ATP	3.7 ± 0.3	560 ± 70	75 ± 4	6.3 ± 0.6
+ ATP	7.42 ± 0.04	48.3 ± 1.4	280 ± 4	3.77 ± 0.17

Fig. 1: Oligomerisation kinetics of CRY1 under blue light and the influence of ATP. nESI-MS spectrum of CRY1 in the dark (grey line) (**a, c**) and under illumination with blue light (blue line) (**b, d**) in absence **(a, b**) and presence of 100 µM ATP (**c, d**). Exposure to blue light leads to oligomerisation of CRY1, and the addition of ATP promotes this process. Time-resolved mass spectrometry measurements of the CRY1 monomer (**e**), dimer (**f**) and tetramer (**g**) in absence and presence of ATP (**h-j**) and the fit (pink line) obtained from the two-step reversible

618 kinetic model (**l**). **k,** Association (highlighted in blue) and dissociation (highlighted in grey) rates obtained from
619 kinetic modelling in presence and absence of 100 µM ATP.

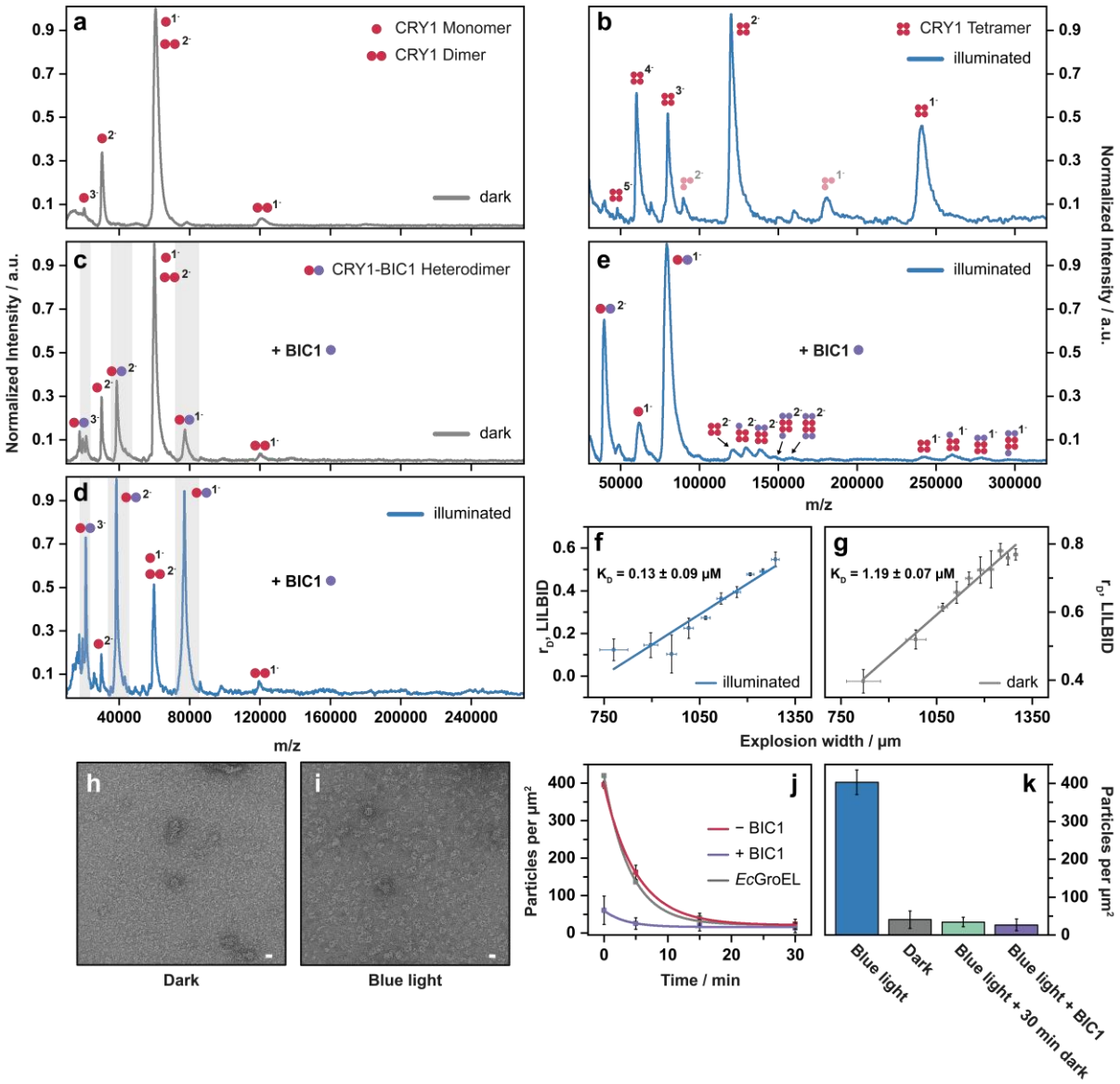

620

621 **Fig. 2: BIC1 inhibits CRY1 oligomerisation in both dark and blue light conditions with higher affinity of**
622 **BIC1 to CRY1 under blue light conditions.** LILBID-MS spectrum of CRY1 shows a monomer (pink dot) (**a**) in
623 darkness, which forms tetramers upon illumination with blue light (**b**). CRY1 trimers are caused by laser
624 dissociation. **c,** Incubation of CRY1 monomer and BIC1 (purple dot) in an equimolar ratio in darkness results in a
625 mixture of CRY1-BIC1 heterodimer and CRY1 monomer. **d,** Upon blue light exposure, the equilibrium shifts
626 towards a higher proportion of the CRY1-BIC1 heterodimer relative to the CRY1 monomer (highlighted in grey).
627 **e,** Under blue light conditions, addition of BIC1 to the CRY1 tetramer results in binding to each protomer, thereby
628 dissociating the tetramer into CRY1-BIC1 heterodimers. **f**, qLILBID-MS measurements reveal that the CRY1-BIC1
629 heterodimer exhibits a ten-fold higher affinity under blue light compared to its dark-state counterpart (**g**). TEM
630 images of CRY1 particles visualised by negative staining of probes kept in darkness (**h**), or treated with blue light
631 (450 nm, 20 min, 115 µmol m ^{2} s^{-1}) (**i**) showing light-induced formation of doughnut-like ring structures of CRY1.
632 Scale bars 10 nm. **j**, Kinetics of CRY1 monomerization (n = 3 ± SD) after transfer of samples from blue light to
633 darkness in absence and presence of BIC1 or *E. coli* GroEL as negative control. **k**, Effect of BIC1 on kinetics of

decrease in number of CRY1 particles showing monomerization of CRY1 (n = 3 ± SD). Blue light (465 nm, fluence rate 115 µmol m^{-2} s^{-1}) treatment was for 20 min.

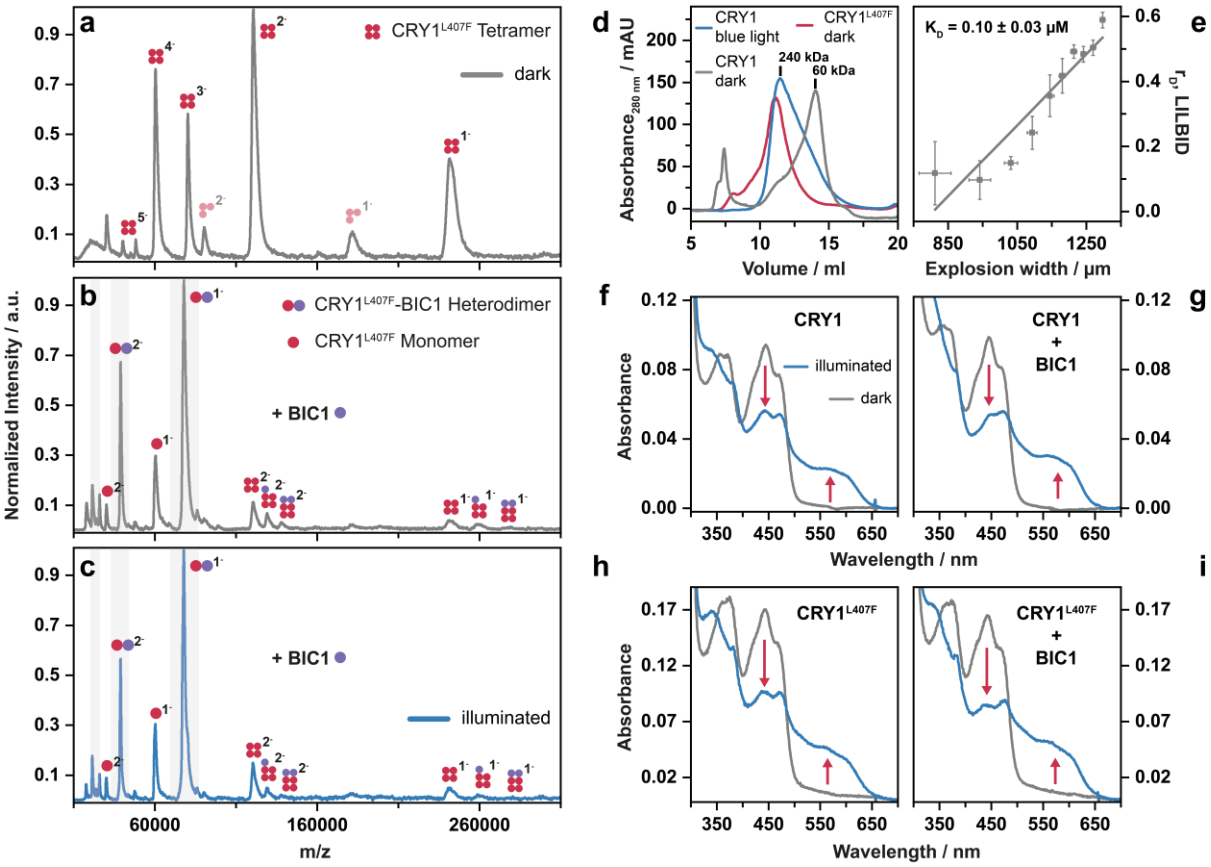

Fig. 3: BIC1 disassembles constitutively active CRY1 tetramers and does not inhibit photoreduction of the FAD cofactor. a, LILBID-MS spectrum of the constitutively active $CRY1^{L407F}$ mutant shows a tetramer in darkness. CRY1 trimers are caused by laser dissociation. **b**, Addition of BIC1 (purple dot) to $CRY1^{L407F}$ in an equimolar ratio in darkness results in binding to each protomer, thereby dissociating the $CRY1^{L407F}$ tetramer into $CRY1^{L407F}$-BIC1 heterodimer and monomeric $CRY1^{L407F}$. **c**, Exposure to blue light does not shift the equilibrium toward the $CRY1^{L407F}$-BIC1 heterodimer, as has been shown for wild-type CRY1. **d**, SEC elution profiles of wild-type CRY1 kept in darkness or irradiated with blue light, and of hyperactive $CRY1^{L407F}$ mutant kept in darkness. **e**, qLILBID-MS measurement of the $CRY1^{L407F}$-BIC1 heterodimer under dark conditions revealed that BIC1 binds $CRY1^{L407F}$ with high affinity. **f**, Absorption spectra of wild-type CRY1 before (grey line) and after (blue line) blue light exposure indicate FAD photoreduction, with a decrease in FAD_{ox} peak at 450 nm, and the emergence of a broad band at 550-600 nm, characteristic for the FADH° semiquinone. **g**, Addition of BIC1 to wild-type CRY1 does not inhibit the photoreduction of CRY's FAD chromophore. **h**, Absorption spectra of the $CRY1^{L407F}$ mutant indicates that chromophore photoreduction remains unaffected by the mutation. **i**, Photoreduction of the FAD chromophore in the $CRY1^{L407F}$ mutant remains unaffected by BIC1 addition, as observed for wild-type CRY1.

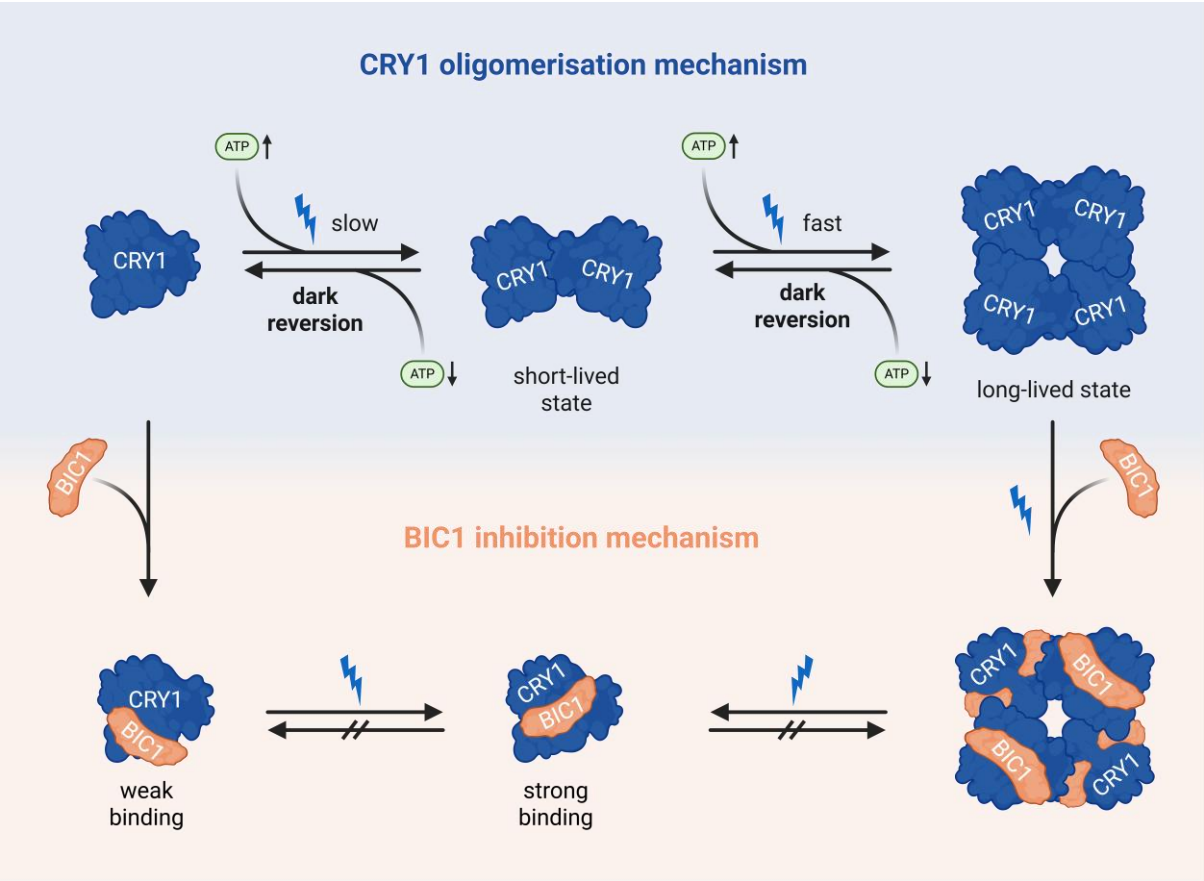

Fig.4: Schematic model of CRY1 oligomerisation dynamics, ATP modulation, and BIC1-mediated inhibition. Upon blue light exposure, CRY1 transitions from a monomeric to a tetrameric state via a short-lived dimeric intermediate. This oligomerisation follows a sequential, reversible two-step mechanism. ATP enhances the association rates for dimer and tetramer formation, while slowing down the dissociation rates of these oligomers. BIC1 binds CRY1 in both dark and light conditions, with significantly higher affinity for the light-activated conformation. This interaction prevents oligomer formation and actively disassembles pre-formed tetramers by binding to individual CRY1 protomers even under continuous blue-light illumination.